Accepted Manuscript

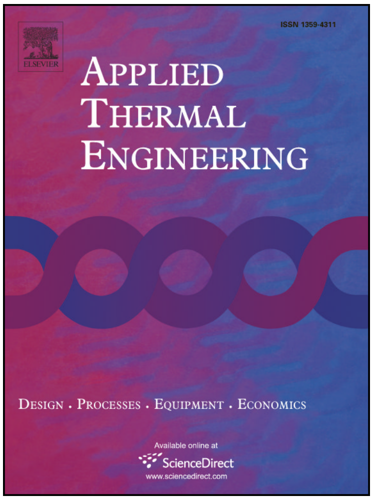

The Effect of Ambient Pressure on the Heat Transfer of a Water Spray

Tiago Costa, Jorge Martins, F.P. Brito, Miguel R. Oliveira Panão, Antóio L.N. Moreira

PII: S1359-4311(18)36409-3
DOI: https://doi.org/10.1016/j.applthermaleng.2019.02.089
Reference: ATE 13383

To appear in: *Applied Thermal Engineering*

Received Date: 19 October 2018
Accepted Date: 17 February 2019

Please cite this article as: T. Costa, J. Martins, F.P. Brito, M.R. Oliveira Panão, A.L.N. Moreira, The Effect of Ambient Pressure on the Heat Transfer of a Water Spray, *Applied Thermal Engineering* (2019), doi: https://doi.org/10.1016/j.applthermaleng.2019.02.089

The Effect of Ambient Pressure on the Heat Transfer of a Water Spray

Tiago Costa[a,*], Jorge Martins[b], F. P. Brito[b], Miguel R. Oliveira Panão[c], António L.N. Moreira[d]

[a] *MIT Portugal – EDAM, University of Minho, School of Engineering, Campus de Azurém, 4800-058 Guimarães, Portugal*
[b] *MEtRICs, University of Minho, Mechanical Engineering Dept., Campus de Azurém, 4800 Guimarães, Portugal*
[c] *ADAI-LAETA, Mechanical Engineering Department, University of Coimbra, Rua Luis Reis Santos, 3030-788 Coimbra, Portugal*
[d] *IN+, Mechanical Engineering Department, Instituto Superior Técnico, University of Lisbon, Av. Rovisco Pais, 1049-001 Lisboa, Portugal*

Abstract

The present work is aimed at quantifying the effects of ambient pressure in the heat transfer at single injections of a full cone spray over a hot metal surface. The experimental configuration is that of a spray impinging down perpendicularly onto a flat surface located at 55 *mm* inside an injection chamber. The experiments were conducted for prescribed initial wall temperatures ranging from single phase to local nucleate boiling and transition regimes of heat transfer. Ambient pressures ranged from atmospheric to 30 *bar*. The analysis is based on spatial resolved measurements of the instantaneous surface temperature during the injection period. The measurements are then

---

[*] Corresponding author

Email addresses: `id5739@alunos.uminho.pt` (Tiago Costa), `jmartins@dem.uminho.pt` (Jorge Martins), `francisco@dem.uminho.pt` (F. P. Brito), `miguel.panao@dem.uc.pt` (Miguel R. Oliveira Panão), `aluismoreira@tecnico.ulisboa.pt` (António L.N. Moreira)

Preprint submitted to Applied Thermal Engineering *February 18, 2019*

processed in order to obtain estimates of the time-averaged values of the local heat flux. The overall cooling rate is also obtained by integrating the local values within the total area of the spray impact. Results show that the amount of heat extracted by the impinging spray increases 3.4 times when ambient pressure is increased from atmospheric to 20 *bar* at the same superheating degree at the wall of 45 $^\circ C$. This corresponds to an increase from 13.3 % to 47.7 % in the ratio between the actual cooling and the theoretical maximum cooling, defined here as cooling efficiency. This is a result of a better spreading of the liquid film at the wall, covering a larger footprint upon impact . Instantaneous peak heat flux is also increased, as a clear indication of the improved heat transfer between the impinging droplets and the wall.

The work presented herein derives from a broader research program devised to develop a system for in-cylinder cooling of internal combustion engines using high pressure water sprays produced by gasoline direct injectors.

Keywords: Spray cooling, Transient wall heat flux, High Ambient Pressure

1. Introduction

Cooling at high heat fluxes has been a driver in the development of cooling systems for high power density devices such as nuclear reactors, and a big variety of electronic systems or devices [1]. An advantage of spray cooling systems is the capacity of achieving spatial cooling uniformity and attaining high heat fluxes. Once the spray impinges on the surface, the vaporization of the deposited liquid is a way to achieve a fast removal of heat from small areas [2]. In some occasions, two-phase spray impingement is capable of attaining high heat fluxes due to the high rate of surface re-wetting [3]. And even if the liquid film at the surface is in the Leidenfrost regime, the droplet's momentum is likely to allow it to penetrate the vapour layer and enhance heat transfer.

In fact, the rate of surface cooling of any two-phase cooling system depends on both the rate of liquid vaporization and the rate of removal of vapour from the surface. The advantage of using a spray is that it allows the optimization of the amount of liquid getting into contact as well as the time of contact with the surface, at the same time that inter-droplet space helps vapour to diffuse away from the surface. Of course, this depends on complex thermo-fluid-dynamic mechanisms of interaction determined by spray characteristics at impact (size, density and velocity), surface properties (material, surface energy) and temperature, as shown by Moita and Moreira [4]. The outcome of these mechanisms can be described by different regimes, inferred from overall boiling curves dependant on the injection conditions [5].

The main purpose of the present work, is to analyse the influence of ambient pressure on the heat transfer between the spray droplets and the wall. The outcomes from this study will then be used in the future to validate spray and heat transfer models in order to evaluate and optimize a system for in-cylinder cooling of internal combustion engines using high pressure water sprays produced by gasoline direct injectors. The authors already evaluated the potential for wall heat removal using this strategy in a previous publication [6]. However, information regarding the actual cooling heat flux provided by spray cooling for the range of interest of this application is still missing in literature.

While we may find some experiments at either high or sub-atmospheric ambient pressures for single droplet impacts, or single stationary droplets on a hot surface [7, 8, 9, 10], there is a limited number of experiments focusing on the heat transfer characterization of surface cooling using full sprays under high ambient pressure conditions. Furthermore, the conclusions taken from these experiments are dependent on the conditions and spray characteristics.

In practice, the ambient pressure affects the spray characteristics and, consequently, the spray impingement heat transfer in two ways: droplet size and droplet velocity. Meingast et al. [11] argued that an increase of the injection chamber gas density enhances droplet breakup by aerodynamic effects and produces smaller droplets. These effects explain, according to Meingast et al. [11], the decrease of the heat transfer coefficient at the wall when increasing ambient pressure from 38.5 *bar* to 50 *bar*.

Regarding the effect of ambient pressure on droplet velocity, there is a proportional relation between the droplet velocity just before impinging the surface and the pressure difference between the injection and ambient ($\Delta p = p_{inj} - p_{\infty}$), due to drag forces. This relation further affects the heat transferred when droplets impact on the surface. The results from Issa and Yao [12] and Yan et al. [13], despite being different, point in the same direction. A lower Δp means slower droplets therefore mitigating heat transfer for forced convection of droplets which loose their penetration strength on pre-existing liquid film. However, slower droplets have a lower impact energy, which improves the probability of adhering to the surface or liquid film for a longer period, improving the cooling efficiency [12]. Also from a Thermodynamic point of view, a higher ambient pressure implies a higher saturation temperature and lower latent heat of vaporization, which Issa and Yao [12] correlated with a lower heat transfer coefficient.

Despite the major effects of altering droplet characteristics on heat transfer, Yan et al. [13] also reported how a higher ambient pressure improved nucleate boiling by enhancing the number of active nucleation sites. An increase of the ambient temperature shifts the Leidenfrost regime to higher temperature values, thus, heat transfer occurs closer to the nucleate boiling regime where heat fluxes are higher.

Concluding, there is clearly a lack of experimental research characterizing the transient behaviour of the heat transfer of sprays impinging over hot surfaces under high ambient pressures. For the particular application herein considered, ambient pressures ranging from atmospheric to 30 bar are required. These are typical conditions for combustion chambers of internal combustion engines, where wall surface temperatures of up to $280°C$, require high cooling rates due to the short period available for cooling to occur (less than 20 ms), and therefore, the use of high pressure injectors is required.

The above mentioned analysis, will be performed based on spatial resolved measurements of the instantaneous surface temperature during and shortly after the injection period. The measurements are then processed in order to obtain estimates of the time-resolved of local heat flux. The overall cooling rate is also obtained by integrating the local values within the total area of the spray impact.

Following this introduction, Section 2 explains the measurement techniques and methodologies used for the thermal assessment of the transient and overall cooling process. Sections 2.1 and 2.2 show the calibration and calculation methods used to further analyse and discuss the experimental results in Section 3. The paper ends with a summary of the main concluding remarks.

2. Experimental Procedure and Measurement Techniques

The experimental installation is composed of a custom-built high-pressure injection chamber equipped with a BOSCH HDEV5.2 solenoid type injector using a single-hole with 205 μm in diameter, in combination with a heated target aligned normal to the spray (see Fig. 1). High frequency temperature measurement of the wall surface is accomplished using 5 NANMAC fast-response eroding K-type thermocouples, sampled at 50 kHz.

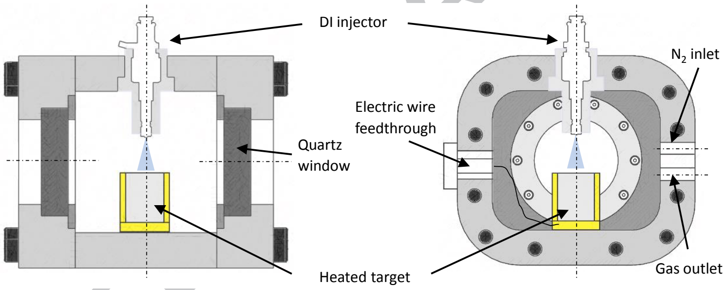

Figure 1: Pressure chamber cross section (a) side view; (b) front view.

The injection chamber is designed to withstand up to 50 bar gas pressure and has optical access at two opposite locations. Ambient pressure inside the chamber and injection pressure were measured using OMEGA PX329 pressure transducers with a total error band of $\pm 1\,\%$.

Nitrogen gas was used in all experiments. The injector was mounted at the top, while the heated target was placed on the bottom at a distance of 55 mm. The wall surface temperatures in the experiments at the start-of-injection ranged from 140 $°C$ to 280 $°C$ and the ambient pressure ranged

Table 1: Thermophysical properties of saturated water for the various ambient pressures tested [14]

Property	**Value at pressure [bar]**			
	1	10	20	30
Saturation temperature ($T_{sat}[^{\circ}C]$)	99.97	179.7	212.2	233.7
Latent heat of vaporization ($h_{fg}[kJ/kg]$)	2257	2014	1889	1794

between atmospheric and 30 bar. The operating parameters that were kept constant throughout the experiments include an injection duration (Δt_{inj}) of 3 ms and a pressure difference between the injection and ambient pressure ($\Delta p = p_{inj} - p_{\infty}$) of 130 bar. This combination resulted in a measured injection mass (m_{inj}) of 7.9 mg, for all the tested conditions.

Each individual injection was performed always after renewing the chamber gas while relative humidity was monitored to be lower than 10 %. In this way it was considered that the variation in relative humidity during a set of experiments was negligible. The water was pressurized to the target pressures using a MAXIMATOR air driven pump. A NI DIDS-2103 direct injector driver system from National Instruments was used to control the injector solenoid valve. All experiments used distilled water and its relevant thermophysical properties at saturated state are listed in Tab. 1.

Fig. 2 shows the schematics of the temperature data acquisition system and the thermocouple layout within the heated target, with the thermocouple #0 placed at the centre of the block aligned axially with the spray. Spaced radially by 3.75 mm from the centre are three thermocouples, #1, #2 and

#3. The arrangement of these three thermocouples allows for a verification of the symmetry of the cooling event. Two additional thermocouples were placed 7.5 mm and 11.25 mm away from the centre, #4 and #5.

The thermocouples were inserted inside a high tolerance through hole in the heated block, where the measuring end of thermocouple assembly sits flush with the impinging surface, so the thermocouple junction sees direct contact with the water.

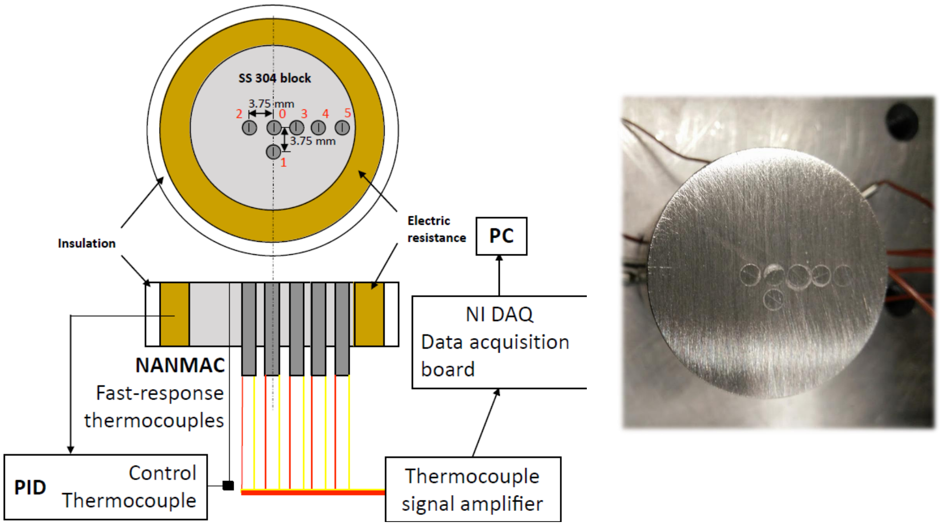

Figure 2: Schematic of the temperature data acquisition system and heated target assembly.

Each thermocouple is composed of a layered configuration of thin foils of alumel, and chromel (K-type) 25 μm thick, insulated by 5 μm thick mica sheets, located in the middle of a AISI Type 304 Stainless Steel tube with an outer diameter of 3.18 mm (Fig. 3). The same material was used in the heated target to avoid errors due to lateral heat conduction, thanks to their similar thermal conductivity. The thermal junction of the thermocouple was formed by rubbing the exposed surface with a #80 grit sand paper before each test, producing multiple microscopic junctions thus allowing for a fast response time of the measured temperature[15, 16, 17] .

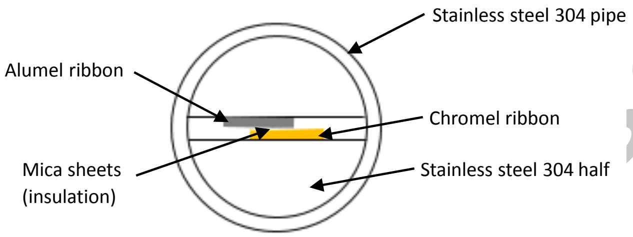

Figure 3: Configuration of the Nanmac fast response thermocouple.

A Phantom Miro 340 high-speed camera used to obtain images of the phenomenon under study had sufficient temporal and spatial resolution to capture the main hydrodynamic structures of spray impact and liquid film formation. The acquisition rate in the experiments was 25,000 FPS, resulting in an image resolution of 320 × 240 px. The images obtained by backlight scattering use the contrast between the liquid and gaseous phases to characterize the outcome of spray impact.

2.1. Thermocouple Calibration Method

Following previous works [18], the calculation of the heat flux based on the resolved wall surface temperature is strongly dependent on how accurately the thermal properties of the junction are known, more specifically the thermal effusivity given by $\beta = \sqrt{k\rho c_p}$.

The effective value of the thermal effusivity for a thermocouple construction will depend on the junction's location, on the chromel or alumel substrate material properties and its proximity to the insulation and housing material. Therefore, each thermocouple must be calibrated before every test, after renewing its thermal junction.

The thermocouple thermal effusivity (β_t), calculated using the contact method, follows a typical heat diffusion problem which arises when two semi-infinite bodies suddenly come into contact. For a certain period of time the contact temperature between the two bodies is constant and depends on their initial temperatures and thermal effusivity [14].

Fig. 4 shows the fast temperature rise T_t, from the initial temperature of the thermocouple T_{init}, to the constant contact temperature $T_{contact}$, by dipping a thermocouple at $T_{init} = 23.7\ ^{\circ}C$ into water at $T_{H_2O} = 50\ ^{\circ}C$. This method is frequently used when calibrating similar thermocouple constructions as can be seen in the following references [15, 16, 17].

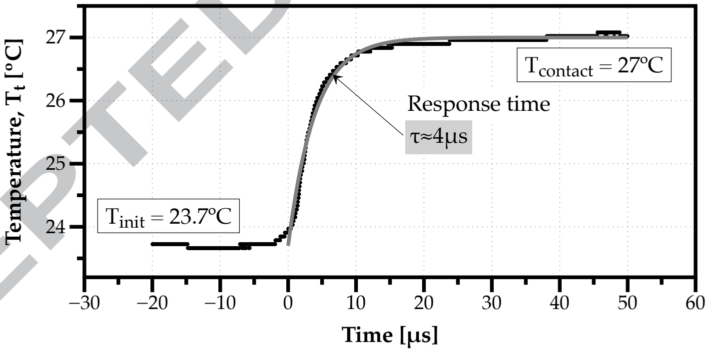

Figure 4: Fast temperature rise from the initial temperature of the thermocouple to the constant contact temperature by dipping a cold thermocouple into a hot liquid. A response time (τ), of 4 μs is obtained using a first-order curve fit.

According to Buttsworth [19], the temperature at the surface of the thermocouple $T_{contact}$ after contact with the water is given by

$$\frac{T_{contact} - T_{init}}{T_{H_2O} - T_{init}} = \frac{\beta_{H_2O}}{\beta_{H_2O} + \beta_t} \qquad (1)$$

The value of β_t can then be calculated from a known value of β_{H_2O}. It is worth to mention that the physical properties of water and the thermocouple vary with temperature. However, the differences are relatively small and the experimentally observed surface temperature is approximately a step function. Thus, it is reasonable to use an effective β_{H_2O} in the equation and the analysis will yield an effective β_t value for the thermocouple.

Figure 5 shows the thermal effusivity β_t value in $J \cdot m^{-2} K^{-1} s^{-1/2}$ for both elements (chromel and alumel, with properties retrieved from Caldwell [20]), and thermocouple calibration results for different tests.

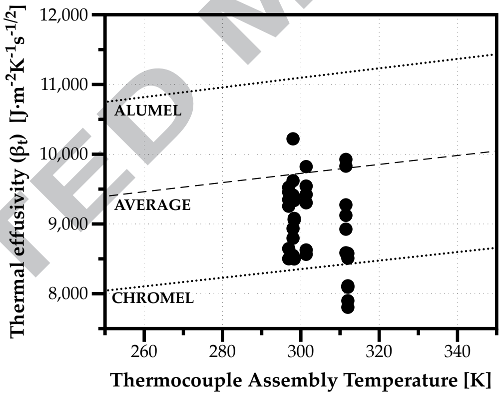

Figure 5: Thermocouple base elements effusivity (β) with varying temperature, and thermocouple calibration results for different tests.

2.2. Heat Transfer Calculation Algorithm

Five individual and separate injection events were performed for each condition. The time-resolved heat flux ($q''_w(t)$) calculated for each injection event uses a MATLAB script to process temperature data obtained for each condition. The uncertainties computed through a standard deviation error analysis are less than 1 % for all experimental tests. Other metrics such as heat transfer rate, heat flux and thermal efficiency, described below, allow for the comparison of the overall performance of the spray at each condition.

The heat flux calculated from temperature data assumes a one-dimensional heat conduction into a semi-infinite body [18]. In ideal conditions, when heat penetrates at the location of the thermocouple, it does not influence the temperature at its opposite end. On the other hand, as explored in a previous work with a similar temperature sensors setup, lateral heat conduction is negligible [21]. Therefore, the one-dimensional heat conduction may apply with good accuracy when measuring fast heat pulses of high heat flux.

Following Panão and Moreira [18], the heat flux can be obtained numerically as

$$q''_w(t) = \frac{2\beta}{\sqrt{\pi}} \sum_{i=1}^{n} \frac{\delta(t_i) - \delta(t_{i-1})}{(t_n - t_i)^{1/2} + (t_n - t_{i-1})^{1/2}} \tag{2}$$

with $\delta(t) = T(t) - T(0)$, as the temperature difference of the thermocouple, recorded during the measurement with respect to the initial temperature.

The time averaged heat flux removed by a single pulse integrates $q''_w(t)$ during the acquisition period or duration (Δt), expressed as,

$$\overline{q''_w}(r, \Delta t) = \frac{1}{\Delta t} \int_0^{\Delta t} q''_w(t) dt \tag{3}$$

The integral is calculated numerically using the composed trapezes rule of integration. Because of the relatively high sample rate, the integration error is negligible.

The overall heat dissipated by the impinging spray is expressed as the integrated spatial variation of heat flux within the total measured area of the spray impact expressed as,

$$\langle \overline{q''_w} \rangle = \frac{2\pi}{A_{impact}} \int_0^R \overline{q''_w}(r, \Delta t) dr \tag{4}$$

Finally, the cooling efficiency is the ratio between the actual cooling and the theoretical maximum cooling, i.e., the ratio of the measured amount of heat extracted by the impinging spray to the maximum that could theoretically be possible to remove from the surface (sensible and latent heat components) for the same initial conditions.

$$\eta_c = \frac{\langle \overline{q''_w} \rangle}{\frac{\dot{m}_f}{A_{impact}} \left[c_{p,f}(T_{f,sat} - T_f) + h_{fg} \right]} \tag{5}$$

3. Results and Discussion

The results presented and discussed in this section consider the effect of ambient pressure on the local and overall transient behaviour of the spray heat transfer upon impact. Before performing any analysis on the effects of heat transfer at the wall, it is possible to draw some conclusions regarding the effect of increasing the chamber pressure on the spray dynamics. Fig. 6 shows a close look of how the instantaneous wall surface temperature varies during the electronic injection duration at the centre of the target ($r = 0\ mm$) for all the ambient pressures tested. Results in Fig. 6 evidence an increase on the spray arrival time, from 0.5 ms at atmospheric pressure up to 1.7 ms at 30 bar.This is a clear indication on how the ambient pressure affects droplet velocity. Spray arrival time is considered when a reduction of more than 2 $°C$ occurs in surface temperature.

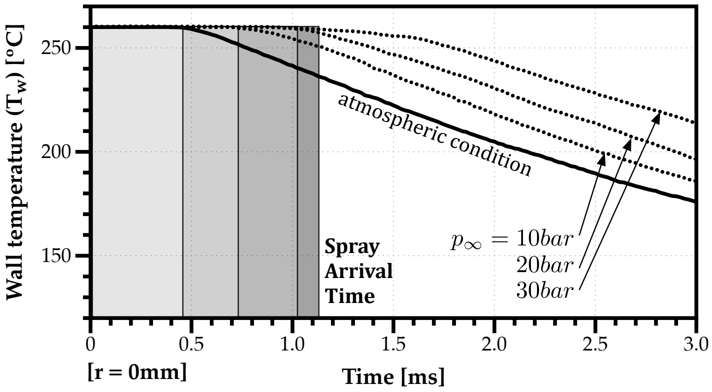

Figure 6: Evolution of surface temperature at $r = 0$ mm for all ambient pressures considered, during electronic injection duration.

Fig. 7 and Fig. 8 show high-speed images of the spray near the wall surface at 2.4 ms and 80 ms after the start-of-injection, respectively, for the full range of chamber pressures tested and a wall temperature of 260 $°C$. At the ambient pressure of 1 bar, despite the observation of a wide range of droplet sizes, this condition shows the presence of the largest droplets of all tested pressure conditions. Also, images allow identifying typical droplet impact hydrodynamic mechanisms such as splash and rebound. In the early stages of spray impact at 1 bar, a significant amount of droplets produced by secondary atomization mechanisms spread randomly in all directions. This outcome represents a poor adhesion of liquid to the heated surface for cooling purposes, resulting from the high impact velocity of spray droplets. When the ambient pressure increases above the atmospheric, images show a gradually higher uniformity degree of droplets with smaller sizes and, consequently, a higher concentration. Later in the cooling process, visualization results show clusters of bubbles typical of nucleated boiling, which generate a thermal induced secondary atomization [22]. The formation of a thermal plume appears as the ambient pressure increases, indicating a high relative degree of saturation near the contact zone (Figure 8).

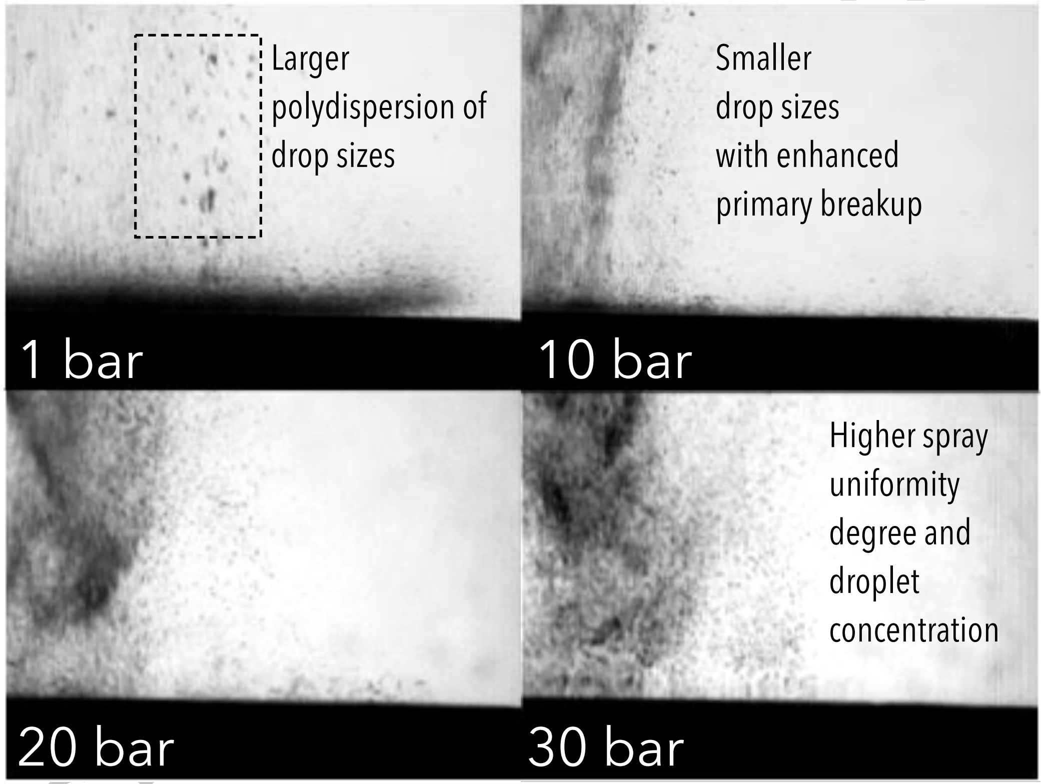

Figure 7: Images taken 2.4 ms after start of injection for 1, 10, 20 and 30 *bar*.

Since the mass of liquid injected is the same, the high concentration of droplets at 10 *bar* point to a clear reduction of their size, intensified for an ambient pressure of 20 *bar* and above. Also, the mechanisms of splash and rebound upon spray impact occur less often, or not at all, and the generation of smaller droplets by thermal induced secondary atomization intensifies for ambient pressures of 20 *bar* and above (see Figure 8).

Finally at 30 *bar*, more droplets adhere to the surface, extending the liquid film covering the surface almost throughout the area captured by the images. The density thermal plume formed above the surface also increases, and propagates from the first stages of spray impact, hindering the layer of liquid formed close to the central axis. The thermal distortion of the nitrogen at the surface is evident and thicker at 20 *bar* and above.

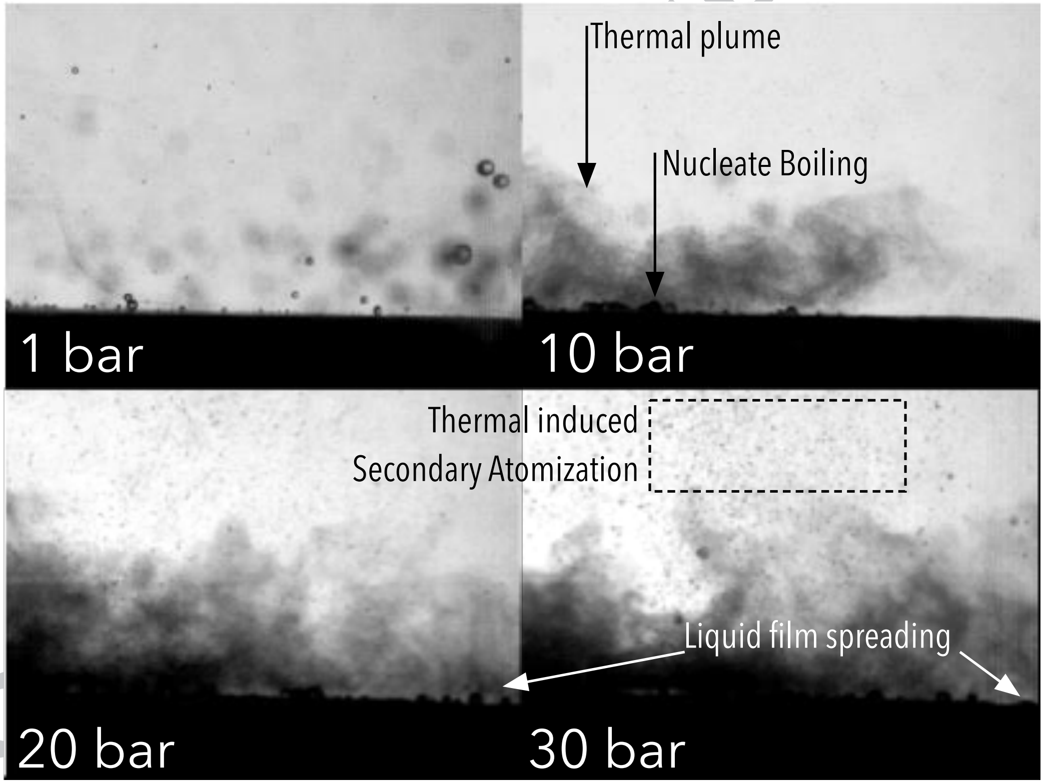

Figure 8: Images taken 80 ms after start of injection for 1, 10, 20 and 30 *bar*.

It is worth to mention that wetting of the chamber walls was only visible for tests performed at atmospheric pressure, clearly indicating a change in the droplets-wall interaction regime. These interactions will play an important role on how the local and global heat transfer varies with ambient pressure, which will be analysed in the following sections.

3.1. Effect of ambient pressure on the local heat transfer evolution

The results depicted in Fig. 9 include the tests performed at a constant initial wall temperature of $T_w(0) = 260\ ^{\circ}C$. Given the effect of the ambient pressure on the saturation temperature, the analysis considers a normalized value of the temperature difference between the wall and the saturation condition (θ) for a better comparison of the results,

$$\theta = \frac{T_w(t) - T_{f,sat}(p_\infty)}{T_w(0) - T_{f,sat}(p_\infty)}$$

It is evident from Fig. 9 that the temperature profiles vary between two limit cases: one which displays a sharp minimum for θ and another one which displays a fairly flat minimum plateau for θ. The former case corresponds to fast surface drying, evidenced when the ambient pressure is increased. The latter case points to a wetted condition, clearly seen at atmospheric pressure. These two limit surface conditions were already evidenced in the work of Labeish [23], and are illustrated in Fig. 10.

For atmospheric pressure, an isothermal plateau between 5 ms and 12 ms, and the lack of cooling for $r \geq 7.5\ mm$, indicates the formation of a liquid film circumscribed by a circular area for $r < 7.5\ mm$. With an increase in pressure, the increasingly sharper behaviour of thermal gradients suggests thinner liquid films due the faster drying of the wall. Thermal gradients also point to the spreading of the liquid film in the radial direction. In fact, Fig. 9

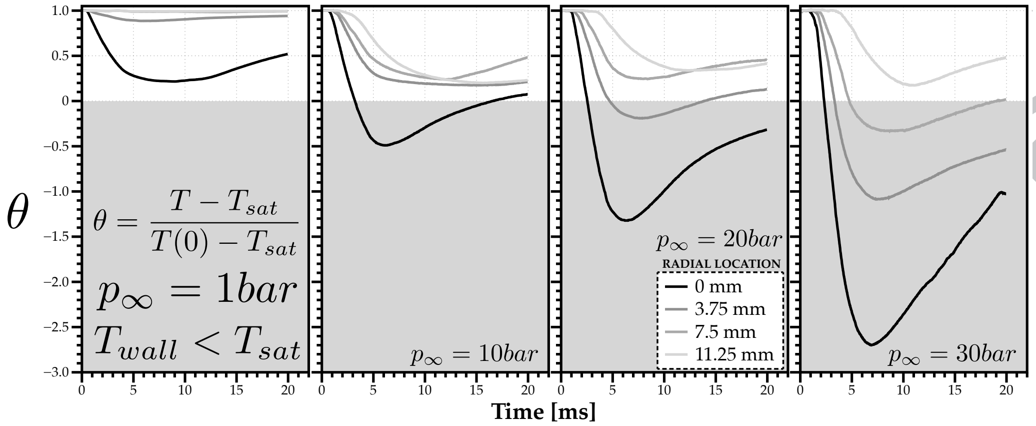

Figure 9: Effect of the ambient pressure on the normalized transient profiles of the temperature difference between the wall and saturation values at different radial locations.

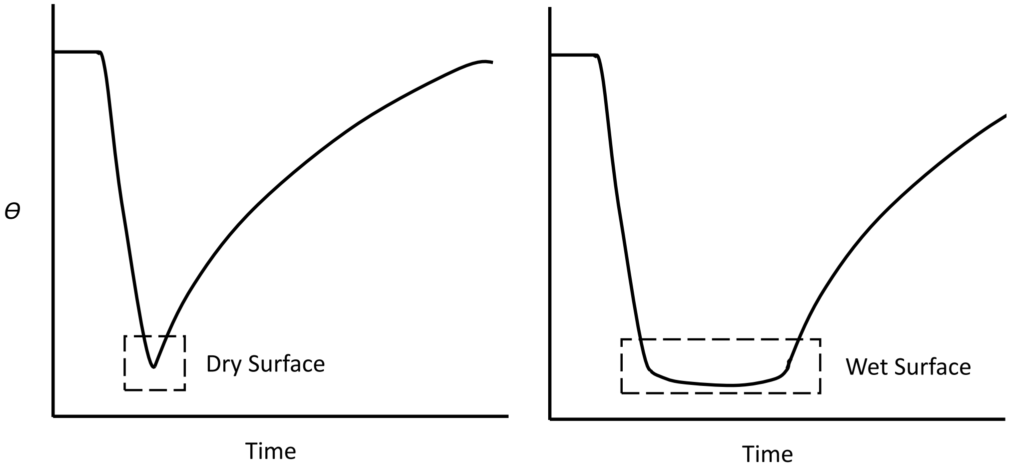

Figure 10: Representation of the behaviour of the normalized wall surface temperature for the two limit surface conditions. Dry surface on the left and wet surface on the right

shows an increasing delay of the θ decay from the centre to the periphery, as the ambient pressure increases, evidencing the presence of a spreading liquid film, covering a larger footprint upon impact.

Table 2: Thermophysical properties of water at $T_w = 260\ ^\circ C$ for the various ambient pressures tested [14]

Property	**Value at pressure [bar]**			
	1	10	20	30
Water temperature ($T_{H_2O}[^\circ C]$)	50.12	53.98	53.69	55.36
Specific Heat at T_{H_2O} ($c_p[J/kgK]$)	4181	4180	4178	4176
Latent heat of vaporization ($h_{fg}[kJ/kg]$)	2257	2014	1889	1794
Jacob Number, Ja	0.092	0.261	0.351	0.415

Considering the effect of ambient temperature on the thermophysical properties, Table 2 synthesis the values assumed in the experiments for constant surface temperature condition at the beginning of each injection ($T_w(0) = 260\ ^\circ C$). The table also includes the values of the Jakob number for each test, ($\text{Ja} = \frac{c_{p,f}(T_{sat}-T_f)}{h_{fg}}$) which relates the sensible to the latent heat of the injected mass. This number is a measure of the relative importance between a single-phase heat transfer, depending mostly on the sensible heat, and two-phase heat transfer, which depends mostly on the latent heat.

It is reasonable to argue that the Jakob number may justify the difference observed between the results at atmospheric pressure and the other pressures. In atmospheric conditions, a lower Jakob points to the dominant effect of a two-phase heat transfer. However, with a higher ambient pressure, the Jakob number increases by two to four times, which means single-phase heat transfer begins dominating heat exchange in the spray cooling event.

Figure 11 shows the calculated heat flux using Eq. 2, from the measured wall temperature on Fig. 9. Dashed lines evidence how the peak heat flux varies with an increase in ambient pressure, for the different radial locations.

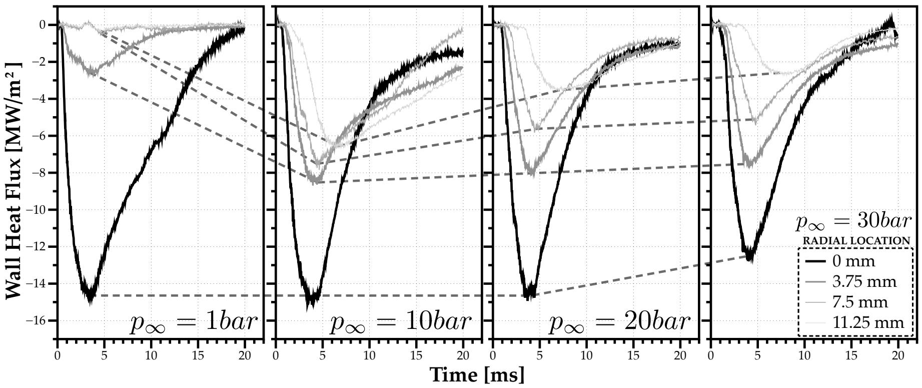

Figure 11: Effect of the ambient pressure on the transient profiles of the surface heat flux for 260 $^\circ C$ at different radial locations.

The sharp decrease on the local heat flux depicted in Fig. 11, especially at $r = 0\ mm$, evidences a fast vaporization of the leading droplets, as reported by Chen and Hsu [24], reaching an absolute maximum. At atmospheric pressure the measured heat flux peak close to 15 MW/m^2 is of the same order of magnitude as the values reported in previous works for two phase high pressure spray cooling and two phase jet impingement, 12 MW/m^2 [25] and 18 MW/m^2 [26], respectively.

Fig. 12 shows an overview of the aforementioned trends, representing the time averaged heat flux at the different wall locations within the area of impact at constant wall temperature.

Under a higher pressure environment, the drag forces exerted in the spray droplets through their interaction with the quiescent surrounding would lower

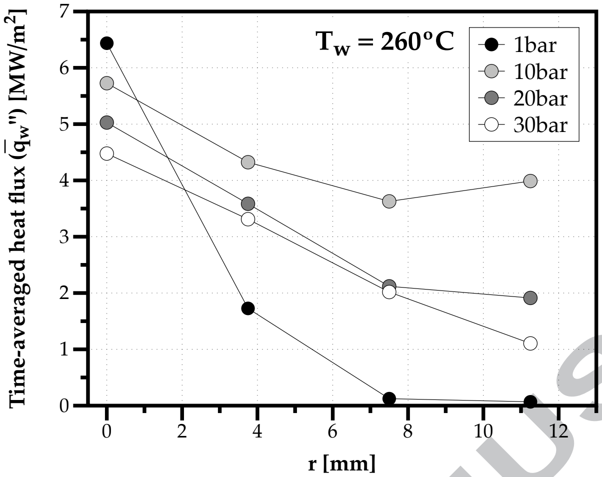

Figure 12: Radial profile of the time average wall heat flux for $T_w = 260$ °C.

their velocity at impact. This favours the deposition of liquid for cooling purposes and the spreading of this film over a larger area, compared to the atmospheric pressure case, justifying the overall heat transfer enhancement from 1 *bar* to 10 *bar*. However, as the ambient pressure further increases, the probability of accumulating liquid, and the lower penetration of impinging droplets onto this film due to their lower velocity, would decrease the convective heat transfer mechanism, as observed in Fig. 12 for 30 *bar*.

The next analysis compares the heat transfer outcomes for different ambient pressures while keeping the difference from the initial wall surface temperature and the water saturation temperature at the respective ambient pressure, here called as superheating degree ($\Delta T_{w-sat} = T_w(0) - T_{sat}$), constant at around 45 °C. This corresponds to $T_w = 145$ °C at atmospheric pressure, $T_w = 225$ °C at 10 *bar*, $T_w = 260$ °C at 20 *bar*, and $T_w = 280$ °C at 30 *bar*.

Compared to the outcomes observed at constant initial wall temperature, the results presented in Fig. 13 are significantly different for all the tested ambient pressure conditions. The peak heat flux increases at the centre location with increasing in ambient pressure up to 20 bar.

Fig. 13 also shows that the temperature drops to below saturation temperature in many of the tested conditions, although temperature profiles are similar for $p_\infty > 10\ bar$. The results at the outer region of the spray qualitatively resemble the observations made at constant wall temperature shown in Figures 9 and 11.

Fig. 14 shows the time averaged heat flux at the different wall locations within the area of impact for the same constant superheating degree of $\Delta T_{w-sat} = 45\ ^\circ C$. It is clear that there is a relevant improvement on the heat transfer capability of the spray when pressure is increased above the atmospheric pressure for the same superheating degree. This is consistent with the work reported by Yan et al. [13] where an increase of the ambient pressure toward values above the atmospheric pressure enhances nucleate boiling.

From the point of view of system performance it is also important to consider the total cooling rate, relatively to the theoretical maximum possible, to account for the complex interactions induced by spatial heterogeneity. This is addressed in the following section.

3.2. Effect of ambient pressure on the overall cooling efficiency

The time averaged heat flux has been integrated within the area of impact given by Eq. (4). Fig. 15 (a) shows the results as a function of the ambient pressure for the two cases (fixed surface temperature and fixed superheating

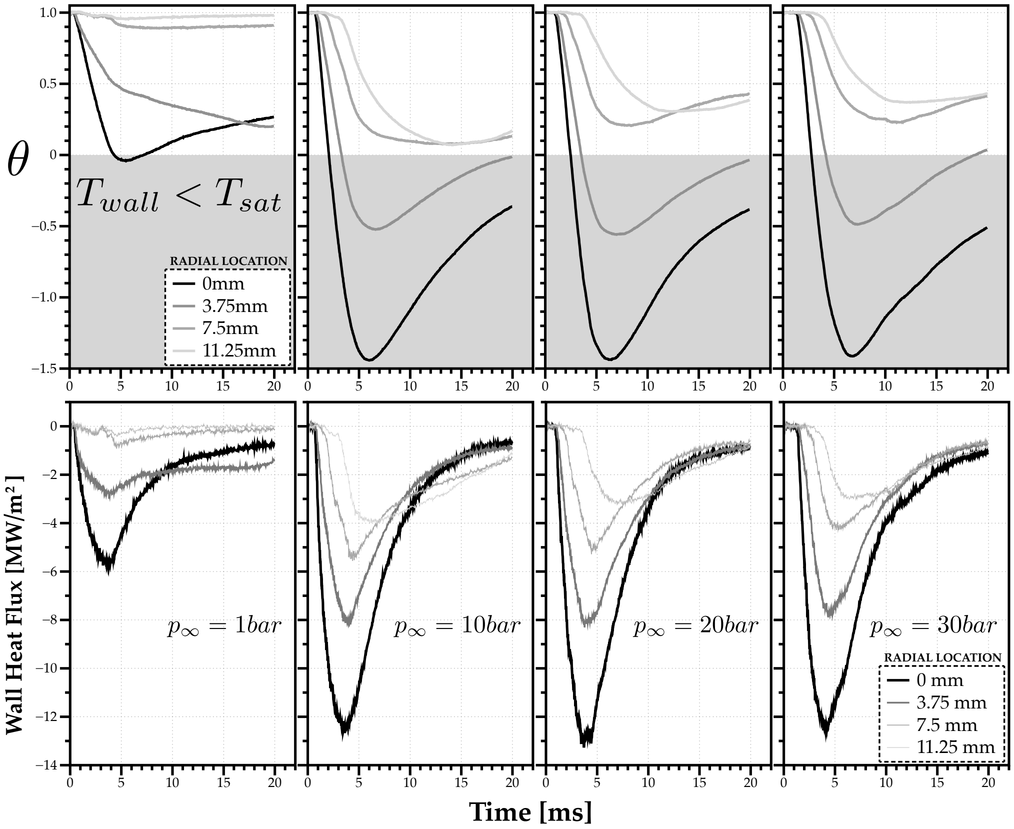

Figure 13: Effect of the ambient pressure on the transient profiles of the surface temperature and heat flux for $\Delta T_{w-sat} = 45$ °C at different radial locations.

degree). Fig. 15 (b) depicts the values of the Jakob number for the analysed cases.

Even if not in magnitude, there is a consistent result when comparing the overall heat dissipation and the Jakob number. Namely, a lower Jakob points to a higher importance of phase-change on the heat removal, which corresponds to the higher heat dissipation in the constant initial temperature condition.

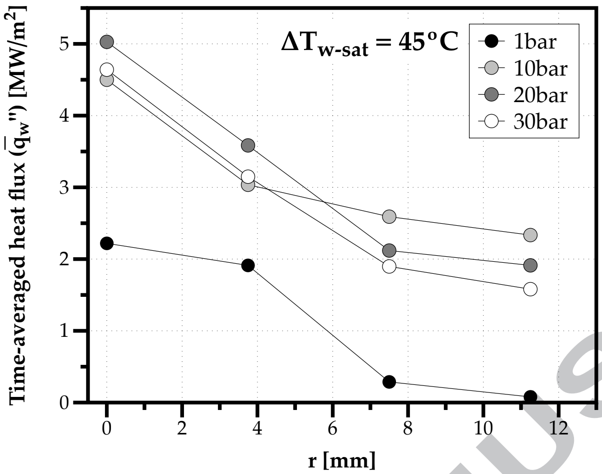

Figure 14: Radial profile of the time average wall heat flux for $\Delta T_{w-sat} = 45\ °C$.

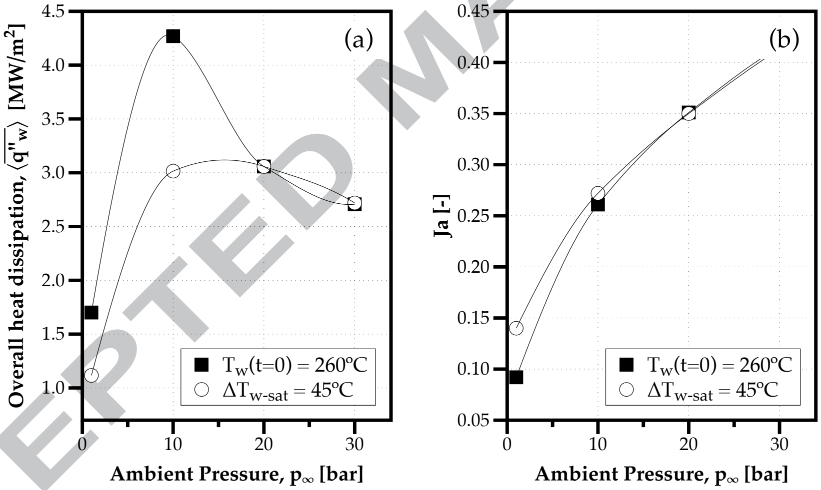

Figure 15: Effect of the ambient pressure on the overall heat flux (a) and corresponding Jakob numbers (b).

For the fixed wall temperature condition, the heat removal is significantly higher at an ambient pressure of 10 *bar* as a result of the higher and more uniform cooling heat fluxes distribution in the radial direction (Fig. 11). In fact, analysing the results obtained for the cooling efficiency (Fig. 16), the higher heat dissipation recorded in Fig. 15 also corresponds to the operating condition of highest cooling efficiency, i.e. possibly the one closer to the Critical Heat Flux (CHF).

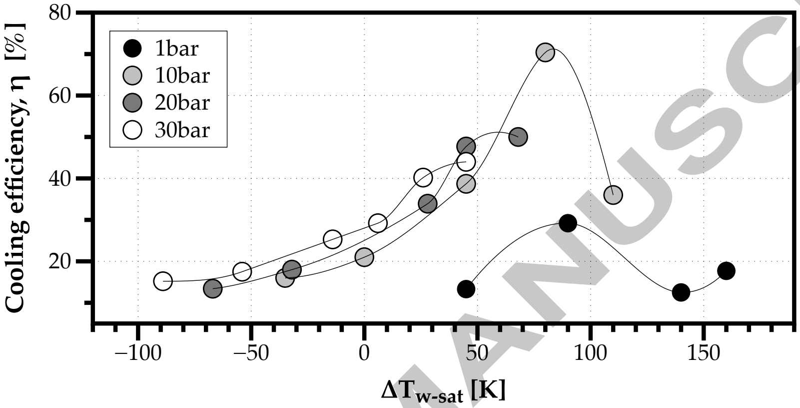

Figure 16: Variation of overall cooling efficiency with superheating degree for the tested ambient pressures.

Generally, the results obtained for the cooling efficiency clearly show the effect of ambient pressure in shifting the curve to lower superheating degree values.

4. Summary and Concluding Remarks

The present work was aimed at providing further insight into the effects of the ambient pressure on the cooling performance of a full cone high-pressure water spray. The experimental configuration consisted of a water spray impacting down perpendicularly onto a heated flat steel wall located at 55 *mm*. The experiments were conducted at prescribed ambient pressures ranging from atmospheric to 30 *bar* and allowed detailed spatial measurements of the instantaneous surface temperature during the period of injection leading to the calculation of the instantaneous heat flux. Testing conditions include initial wall temperatures ranging from 140 $^\circ C$ to 280 $^\circ C$. The injected mass was kept constant at $m_{inj} = 7.9\ mg$ by using an injection duration of 0.3 ms and maintaining a constant pressure difference of 130 bar between the injection and the ambient pressure.

The first analysis assessed the effect of ambient pressure on the heat transfer at a constant initial wall temperature. For the tested conditions, the instantaneous heat flux peak occurred for an ambient pressure of 10 bar. For higher pressures, the lower heat dissipation rate was a clear indication of an interaction between the spray droplets and the increased gas density. The experiments at constant superheating degree showed an evident improvement in the heat flux as ambient pressure increased from atmospheric up to 20 bar. This rise suggests an enhancement of convection heat transfer relatively to nucleate boiling and full film boiling.

Generally, the results reflect the interaction between opposing effects occurring at different ambient pressures. On one hand, lower ambient pressures more easily induce a strong superheating degree which facilitates boiling up to the critical heat flux conditions. On the other hand, higher ambient pressures induce a broader spray angle, which reduces the formation of a thick liquid layer which will hamper heat transfer.

In the second and final analysis, the evaluation of the overall spray cooling performance was achieved by the integration of the time-averaged heat flux over the entire area of impact. The results showed an increase of the cooling efficiency as pressure increased, as long as the critical heat flux is not achieved. Namely, the amount of heat extracted by the impinging spray increased 3.4 times from atmospheric to 20 *bar* at the same superheating degree at the wall of 45°C, improving the cooling efficiency from 13.3 % to 47.7 %.

The results obtained are highly valuable for the exploration of the concept of regenerative cooling in internal combustion engines. This concept enables simultaneously the internal cooling of engines through direct water injection and the recovery of part of the energy lost to cooling through the expansion of the generated vapour. The present work provides invaluable data on spray cooling heat fluxes for a pressure range that was hitherto unavailable. The time scale and magnitude of the heat fluxes measured seems to be suitable for the intended application.

5. Acknowledgments

The authors would like to acknowledge LiquidPiston INC. for providing all the laboratorial conditions to perform the experiments, MEtRICs - Mechanical Engineering and Resource Sustainability Centre (UID/EMS/04077/2019), and Diogo Ferreira for aiding in the high-speed visualization setup and experiments. T. Costa is supported by the Portuguese Foundation for Science and Technology (FCT) under the PhD grant PD/BD/l05929/2014, MIT Portugal Program, and F.P. Brito is supported by FCT under the Post doctoral grant SFRH/BPD/89553/2012 and J Martins is supported by the FCT grant SFRH/BSAB/142994/2018, financed by FEDER funds through Programa Operacional Fatores de Competitividade – COMPETE and National funds through PIDDAC and FCT.

References

[1] W. R. Z. C. Lamini, O., Z. Xu, Enhanced heat spray cooling with a moving nozzle, Applied Thermal Engineering 141 (2018) 921–927.

[2] F. C. Y. C. M. C. Nianyong, Z., W. Yu, Enhanced heat spray cooling with a moving nozzle, Applied Thermal Engineering 141 (2018) 921–927.

[3] B. Horacek, K. T. Kiger, J. Kim, Single nozzle spray cooling heat transfer mechanisms, International Journal of Heat and Mass Transfer 48 (8) (2005) 1425–1438.

[4] A. S. Moita, A. L. N. Moreira, Scaling the effects of surface topography in the secondary atomization resulting from droplet/wall interactions, Experiments in Fluids 52 (2012) 679–695.

[5] C. J. Moreira, A.L.N., M. Panão, An experimental methodology to quantify the spray cooling event at intermittent spray impact, International Journal of Heat and Fluid Flow 28 (2007) 191–202.

[6] T. Costa, J. Martins, F. Brito, Assessment of the potential for wall heat removal by in-cylinder water injection in internal combustion engines, in: ECOS 2018 - The 31st International Conference on Efficiency, Cost, Optimization, Simulation and Environmental Impact of Energy Systems, June 17-22, Guimarães, Portugal, 2018.

[7] G. S. Emmerson, The effect of pressure and surface material on the leidenfrost point of discrete drops of water, International Journal of Heat and Mass Transfer 18 (3) (1975) 381–386.

[8] G. S. Emmerson, C. W. Snoek, The effect of pressure on the leidenfrost point of discrete drops of water and freon on a brass surface, International Journal of Heat and Mass Transfer 21 (8) (1978) 1081–1086.

[9] P. Testa, L. Nicotra, Influence of Pressure on the Leidenfrost Temperature and on Extracted Heat Fluxes in the Transient Mode and Low Pressure, Journal of Heat Transfer 108 (4) (1986) 916–921.

[10] P. J. Halvorson, On the heat transfer characteristics of spray cooling, Ph.D. thesis, Georgia Institute of Technology (1994).

[11] U. Meingast, L. Reichelt, U. Renz, Measuring transient wall heat flux under diesel engine conditions, International Journal of Engine Research 5 (5) (2004) 443–452.

[12] R. J. Issa, S. C. YAO, A Numerical Model for the Mist Dynamics and Heat Transfer at Various Ambient Pressures, Journal of Fluids Engineering 127 (4) (2005) 631–9.

[13] Z. B. Yan, K. C. Toh, F. Duan, T. N. Wong, K. F. Choo, P. K. Chan, Y. S. Chua, Experimental study of impingement spray cooling for high power devices, Applied Thermal Engineering 30 (10) (2010) 1225–1230.

[14] T. L. Bergman, F. P. Incropera, Fundamentals of heat and mass transfer, John Wiley & Sons, 2011.

[15] A. C. Alkidas, Heat Transfer Characteristics of a Spark-Ignition Engine, Journal of Heat Transfer 102 (2) (1980) 189–193.

[16] J. A. Gatowski, M. K. Smith, A. C. Alkidas, An experimental investigation of surface thermometry and heat flux, Experimental thermal and fluid science 2 (3) (1989) 280–292.

[17] Y. M. Qiao, S. Chandra, Boiling of droplets on a hot surface in low gravity, International Journal of Heat and Mass Transfer 39 (7) (1996) 1379–1393.

[18] M. R. O. Panão, A. L. N. Moreira, Intermittent spray cooling: A new technology for controlling surface temperature, International Journal of Heat and Fluid Flow 30 (1) (2009) 117–130.

[19] D. R. Buttsworth, Assessment of effective thermal product of surface junction thermocouples on millisecond and microsecond time scales, Experimental thermal and fluid science 25 (6) (2001) 409–420.

[20] F. R. Caldwell, Thermocouple materials, National Bureau of Standards, 1962.

[21] A. L. N. Moreira, M. R. O. Panao, Heat transfer at multiple-intermittent impacts of a hollow cone spray, International Journal of Heat and Mass Transfer 49 (21-22) (2006) 4132–4151.

[22] J. Breitenbach, I. V. Roisman, C. Tropea, From drop impact physics to spray cooling models: a critical review, Experiments in Fluids 59 (3) (2018) 418.

[23] V. G. Labeish, Thermohydrodynamic study of a drop impact against a heated surface, Experimental thermal and fluid science 8 (3) (1994) 181–194.

[24] J. C. Chen, K. K. Hsu, Heat Transfer During Liquid Contact on Superheated Surfaces, Journal of Heat Transfer 117 (3) (1995) 693–697.

[25] M. R. Pais, L. C. Chow, E. T. Mahefkey, Surface Roughness and Its Effects on the Heat Transfer Mechanism in Spray Cooling, Journal of Heat Transfer 114 (1) (1992) 211.

[26] M. R. Overholt, A. McCandless, K. W. Kelly, C. J. Becnel, S. Motakef, Micro-Jet Arrays for Cooling of Electronic Equipment, ASME 3rd International Conference on Microchannels and Minichannels (2005) 249–252.

Highlights about the research paper, entitled “*The Effect of Ambient Pressure on the Heat Transfer of a Water Spray*” by Tiago Costa (corresponding author), Jorge Martins, Francisco P. Brito, Miguel Panão, and António Moreira.

- An increase of the chamber pressure induces a better liquid film spreading;
- Higher chamber pressures reduce the formation of a thick liquid layer;
- Increasing chamber pressure shifts the boiling curves to lower superheating degrees;
- Thermocouple thermal effusivity variation highlights the value of their calibration.